Relationship between Energetic Disorder and Reduced Recombination of Free Carriers in Organic Solar Cells

Hosseini, Seyed Mehrdad; Wilken, Sebastian; Sun, Bowen; Huang, Fei; Jeong, Sang Young; Woo, Han Young; Coropceanu, Veaceslav; Shoaee, Safa

Published in:
Advanced Energy Materials

DOI:
10.1002/aenm.202203576

Published: 24/02/2023

Document Version
Final published version

Document License
CC BY

ADVANCED ENERGY MATERIALS
www.advenergymat.de

Relationship between Energetic Disorder and Reduced Recombination of Free Carriers in Organic Solar Cells

*Seyed Mehrdad Hosseini, Sebastian Wilken, Bowen Sun, Fei Huang, Sang Young Jeong, Han Young Woo, Veaceslav Coropceanu, and Safa Shoaee**

Reducing non-radiative recombination is key to achieve high fill factors (FFs) in organic solar cells. While it is generally accepted that recombination proceeds via charge transfer (CT) states at the donor:acceptor interface, the underlying principles that dictate the decay kinetics of these CT states are not yet well understood. Here, a study on the effect of energetic disorder is presented. Based on a data set of 10 representative donor:acceptor blends, clear correlations between disorder, the recombination coefficient of free charge carriers, and the non-radiative voltage loss are found. It is suggested that a narrower distribution of CT energies leads to a longer CT decay time and thus reduces non-radiative losses. This leads to a simultaneous improvement of the FF and open circuit voltage and highlights the importance of having materials with low energetic disorder on the way to the commercialisation of organic photovoltaics.

1. Introduction

Non-radiative recombination limits both the open circuit voltage (V_{OC}) and the fill factor (FF) of organic solar cells (OSCs).[1,2] Although some of the losses in FF could be reduced by moving from fullerene to non-fullerene acceptors (NFAs), even the best OSCs still do not reach their full thermodynamic potential.[3] In fact, even in optimized devices with a thin active layer, the FF lags behind what Shockley–Queisser theory predicts for the given V_{OC} values.[4] Moreover, the losses in the FF typically become greater with increasing thickness, which hinders the upscaling of OSCs using low-cost manufacturing based on printing techniques.[5]

The recombination of free charge carriers in OSCs proceeds through charge transfer (CT) states at the interface between the donor (D) and acceptor (A) material. It thus resembles a series of two processes, the carriers' encounter to form a (singlet or triplet) CT state and its subsequent decay to the ground state. The decay is either radiative or non-radiative, with non-radiative pathways typically dominating because of a low CT to ground state oscillator strength.[6] By convention, the total recombination rate constant k_{rec} is often compared with the Langevin coefficient k_L describing charge encounter in a homogeneous medium. Achieving strongly reduced Langevin recombination ($k_{rec} \ll k_L$) is paramount to achieve high FFs, in particular in thick junctions, while simultaneously improving V_{OC}. There is growing consensus that such a situation is realised in blends showing high CT (re-)dissociation yields in which an equilibrium between free carriers and CT states is established.[7–12] The position of the equilibrium is given by the decay of the CT states, mainly through non-radiative pathways.

Despite its importance, the mechanisms of non-radiative decay are not yet well understood. Using Marcus theory, Benduhn et al.[13] proposed the so-called energy-gap law, predicting an exponential dependence of non-radiative recombination on the CT state energy E_{CT}. This was partly challenged by recent studies indicating that non-radiative losses can also be determined by parameters other than E_{CT}, such as electronic couplings of the CT state with the ground state and local D/A excitonic states, as well as electron-vibrational couplings.[14,15] All these studies have in common that they assume a single CT energy, whose spectral features are broadened only by electron-phonon

S. M. Hosseini, B. Sun, S. Shoaee
Optoelectronics of Disordered Semiconductors
Institute of Physics and Astronomy
University of Potsdam
14476 Potsdam-Golm, Germany
E-mail: shoai@uni-potsdam.de

S. Wilken
Physics
Faculty of Science and Engineering
Åbo Akademi University
20500 Turku, Finland

F. Huang
Institute of Polymer Optoelectronic Materials and Devices
State Key Laboratory of Luminescent Materials and Devices
South China University of Technology
Guangzhou 510640, P. R. China

S. Y. Jeong, H. Y. Woo
Department of Chemistry
College of Science Korea University
145 Anam-ro, Seongbuk-gu, Seoul 02841, Republic of Korea

V. Coropceanu
Department of Chemistry and Biochemistry
The University of Arizona
Tucson, AZ 85721-0088, USA

The ORCID identification number(s) for the author(s) of this article can be found under https://doi.org/10.1002/aenm.202203576.

DOI: 10.1002/aenm.202203576

coupling, also known as a dynamic disorder. In an organic blend, however, the weak cohesion between individual molecules through van der Waals interactions together with conformational irregularities lead to a broadened distribution of CT states rather than a single E_{CT}, which is referred to as static disorder. Static disorder is well known to result in dispersive charge transport, but its relevance for charge generation and recombination remains controversial.[16–25] Recently, Yan et al.[26] demonstrated for two particular polymer:NFA blends the importance of accounting for CT-state static disorder in analysing voltage losses. This observation raises the question of how non-radiative recombination is generally affected by energetic disorder and how this limits the performance of OSCs.

Here, we present a large experimental data set on the effect of disorder on charge recombination based on a range of solution-processed D:A blends comprising both fullerene and NFAs. The overarching aim of this work is the establishment of a general trend for various chemical structures, beyond a specific family of molecules. We establish clear correlations between energetic disorder, the bimolecular recombination coefficient k_{rec} which in turn also correlates with the non-radiative voltage loss (ΔV_{nr}). Our experiments show that our findings are material agnostic within the organic semiconductors and that by reducing the (static) energetic disorder, the recombination of free charge carriers and voltage losses are concurrently suppressed. Based on these findings, we postulate that suppression of free carrier and voltage losses upon decreasing energetic disorder is due to a prolonged CT lifetime, which thus is a key parameter in reducing non-radiative recombination to gain in both V_{OC} and the FF.

2. Results and Discussion

Our study involves D:A blends of five different donors (both polymers and small molecules) with either the fullerene $PC_{71}BM$ or one of four different NFAs. The chemical structures of the materials are depicted in **Figure 1**a and the photovoltaic performance in OSCs is summarised in Table S1 (Supporting Information). For the fullerene-based blends BTR:$PC_{71}BM$ and NT812:$PC_{71}BM$, we induced a change in recombination by varying the D:A ratio and applying solvent vapour annealing, respectively. Previous studies have indicated that such changes affect the blend morphology, in particular the degree of fullerene aggregation.[27,28] For the NFA-based PM6:Y6 blend, we used a similar structure-property relationship based on increasing the solvent additive ratio and thickness.[29] Altogether, this makes a total of ten different photovoltaic systems that are reported on in the following.

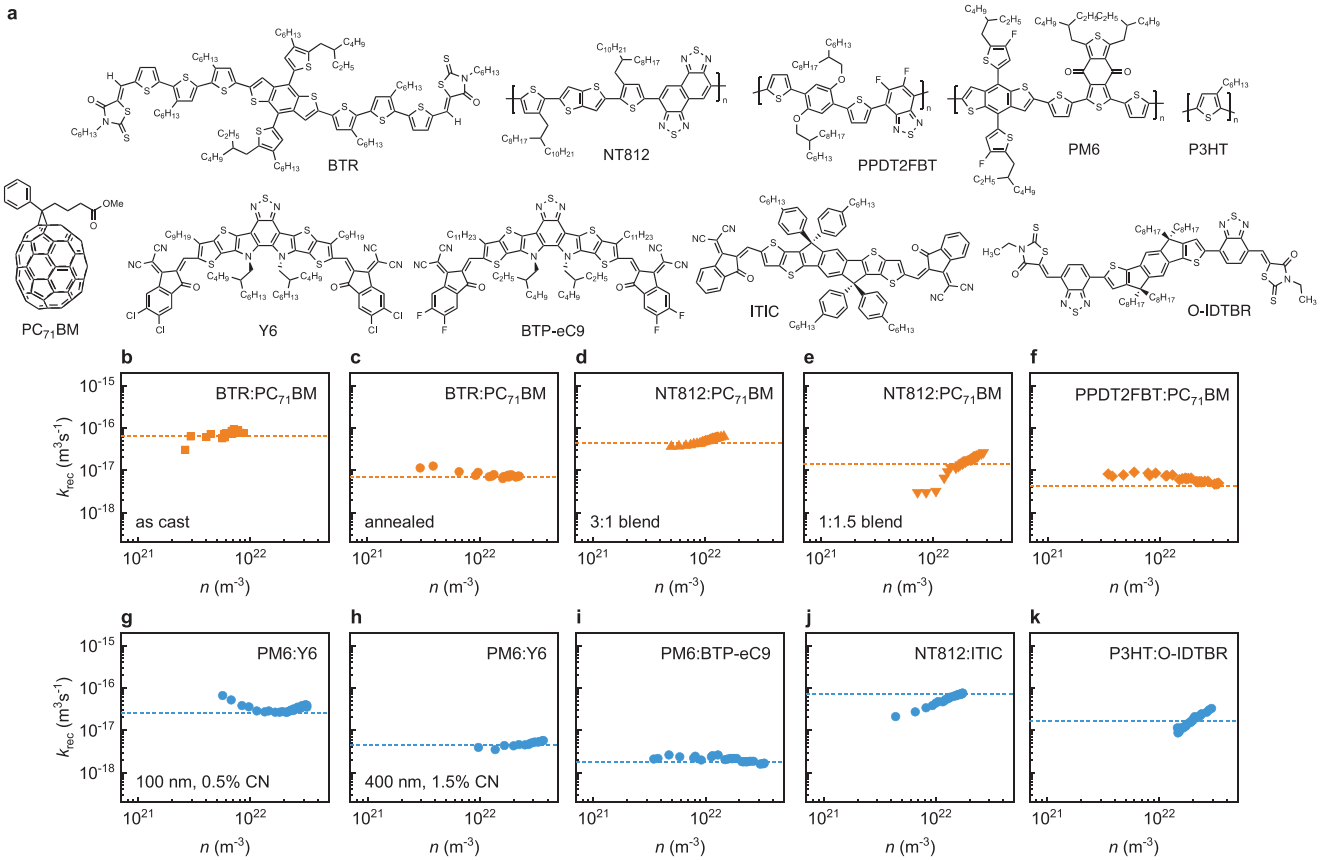

Figure 1. Materials and their charge recombination kinetics in OSCs. a) Molecular structures of the donor (upper row) and acceptor (lower row) materials used in this study. The photovoltaic performance of OSCs based on different D:A blends are summarized in Table S1 (Supporting Information). b–k) Recombination coefficient k_{rec} as a function of the charge carrier concentration n as determined by BACE measurements. The data in b–f) represents devices comprising the fullerene acceptor $PC_{71}BM$ and the data in g–k) represents devices comprising different NFAs. Dashed lines indicate the recombination coefficient under solar illumination.

Figure 1b–k shows the recombination coefficients of photo-generated charge carriers obtained from bias-assisted charge extraction (BACE) measurements as detailed in Note S2 (Supporting Information). With the notable exceptions of NT812:ITIC (Figure 1j) and P3HT:O-IDTBR (Figure 1k), all blend systems exhibit fairly pure second-order kinetics, that is, a recombination rate of the form $R = k_{rec}n^2$, where n is the carrier density and k_{rec} is constant. The higher recombination order in these blends is anticipated to stem from carrier-dependent mobility which affects the carriers' encounter in the recombination process. With k_{rec} ranging from 10^{-18} to 10^{-16} m^3 s^{-1}, the systems investigated span a wide range of recombination strengths that is representative of the state of the art. Next, we studied the charge carrier mobility and energetic disorder from temperature-dependent space charge limited current (SCLC) transport measurements. Figure S1 (Supporting Information) shows the measured current–voltage curves for single-carrier devices and fits the Murgatroyd–Gill model to determine the zero-field mobility μ_0 for electrons and holes.[30] Details of the fitting procedures are given in Note S3 (Supporting Information). We have then applied the Gaussian disorder model (GDM), which assumes that the density of states (DOS) as a result of the energetic disorder can be represented by a Gaussian distribution with the standard deviation σ. According to the GDM, the temperature dependence of the zero-field mobility is given by[30,31]

$$\mu_0(T) = \mu^* \exp\left(-0.44\left(\frac{\sigma}{k_B T}\right)^2\right) \quad (1)$$

where μ^* is the mobility at infinite temperature, and $k_B T$ the thermal energy. We found that Equation (1) describes the temperature dependence of μ_0 for all blend systems within reasonable accuracy (see Figure S1, Supporting Information). The extracted disorder σ_{LUMO} and σ_{HOMO} of the lowest unoccupied molecular orbital (LUMO) of the A and the highest occupied molecular orbital (HOMO) of the D, respectively, are listed in **Table 1**. With σ = 50 to 100 meV, the disorder values span the typical range encountered in organic semiconductors.[30,32,33] Table 1 also includes the reduction factor $\gamma = k_L/k_{rec}$ with the Langevin coefficient calculated using the measured zero-field mobilities at room temperature. Based on γ, the blends can be categorised into Langevin ($\gamma \approx 1$) and non-Langevin systems ($\gamma \gg 1$). For the BTR:$PC_{71}BM$, NT812:$PC_{71}BM$ and PM6:Y6 blends, the changes in preparation conditions described above lead to a change between the two groups.

In the following, we consider the convolution of the DOS site distributions experienced by free electrons and holes, $\sigma_{tr}^2 = \sigma_{HOMO}^2 + \sigma_{LUMO}^2$, as a measure of the CT state disorder relevant for charge recombination. Justification for this approach is given in earlier work[22,32] and also later in the text. **Figure 2**a shows that the device FF clearly shows a generally decreasing trend with increasing disorder. The data show a relatively high scatter as the FF subsumes many device properties including the active-layer thickness. Given that all of the blends studied here exhibit efficient photo-generation, we assume that the general trend of the FF is related to the recombination of free charge carriers through the CT manifold that competes with charge extraction (see Note S4 (Supporting Information) for detailed explanation).[34,35] This is supported by Figure 2b,c, showing that for all samples except for the thin PM6:Y6 device, k_{rec} increases and γ decreases with increasing disorder. Interestingly, whilst the trend in reduction factor and disorder (Figure 2c) is in in line with our previous prediction,[36] our experimental data on the recombination coefficient and energetic disorder are in apparent contradiction to previous studies[37,38] suggesting that charges situated in the tail of the inhomogeneously broadened DOS must be excited back to the transport level to be able to meet the counter charge at the interface. In this picture, higher energetic disorder leads to a barrier for free charge carriers to reform the CT state, which would delay and thereby reduce recombination. On the other hand, lower disorder leads to

Table 1. Key parameters for the blends used in this study.

Active layer	Thickness [nm]	$\mu_{0,n}$ [m^2 V^{-1} s^{-1}]	$\mu_{0,p}$ [m^2 V^{-1} s^{-1}]	σ_{LUMO} [meV]	σ_{HOMO} [meV]	k_{rec} [m^3 s^{-1}]	γ	EQE_{EL}	ΔV_{nr} [V]
BTR:$PC_{71}BM$ (as cast)	290	6.9E-8	2.5E-9	76	71	7.3E-17	5	1.7E-6	0.335
BTR:$PC_{71}BM$ (annealed)	290	1.3E-7	1.3E-7	72	55	7.6E-18	177	3.5E-6	0.320
NT812:$PC_{71}BM$ (3:1)	200	1.8E-8	1.5E-7	67	66	4.9E-17	18	5.7E-7	0.363
NT812:$PC_{71}BM$ (1:1.5)	180	3.0E-7	6.3E-8	59	60	1.6E-17	117	1.4E-6	0.340
PPDT2FBT:$PC_{71}BM$	260	1.3E-7	2.3E-7	63	60	4.8E-18	388	2.6E-6	0.325
PM6:Y6 (100 nm, 0.5% CN)	100	2.1E-8	7.1E-9	58	60	2.9E-17	5	2.6E-5	0.267
PM6:Y6 (400 nm, 1.5% CN)	400	2.6E-7	7.8E-9	50	59	4.9E-18	283	5.1E-6	0.308
PM6:BTP-eC9	80	4.1E-8	2.1E-8	53	60	2.0E-18	160	3.5E-5	0.259
NT812:ITIC	100	1.3E-10	2.5E-8	93	83	8.0E-17	2	3.5E-6	0.317
P3HT:O-IDTBR	180	5.4E-9	2.2E-7	73	61	1.9E-17	61	6.2E-7	0.361

Overview of the measured charge transport and recombination parameters. Charge transport was characterised using temperature-dependent SCLC measurements, see Note S3 (Supporting Information) for details. The listed zero-field mobilities of electrons and holes refer to room temperature. The disorder of the LUMO and HOMO was extracted from the temperature dependence of $\mu_{0,n}$ and $\mu_{0,p}$ according to Equation (1). All SCLC data and fits are shown in Figure S1 (Supporting Information). The recombination coefficient k_{rec} refers to 1-sun illumination and was determined from BACE measurements. The reduction factor $\gamma = k_L/k_{rec}$ was calculated using the Langevin rate constant $k_L = q(\mu_{0,n} + \mu_{0,p})/\varepsilon\varepsilon_0$, where q is the elementary charge and $\varepsilon\varepsilon_0$ the dielectric constant. The voltage loss ΔV_{nr} was calculated from the measured EQE_{EL} using Equation (3). The photovoltaic performance of devices based on the different blends is summarised in Table S1 (Supporting Information).

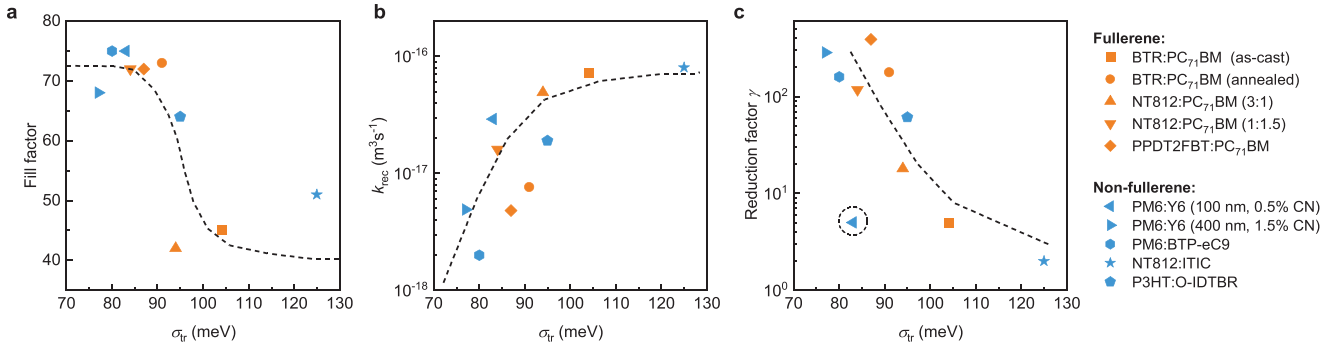

Figure 2. Fill factor and recombination characteristics as a function of disorder a) Device fill factor under solar illumination. Note that the devices had different active-layer thicknesses (see Table 1), which contributes to the scatter of the data.[33] b) Recombination coefficient k_{rec} for a carrier density corresponding to solar illumination. c) Langevin reduction factor $\gamma = k_L/k_{rec}$, where k_L is the Langevin recombination coefficient calculated with the zero-field mobilities given in Table 1 and assuming a relative dielectric constant of 3.5. The abscissa is the convolution of the disorder values σ_{LUMO} and σ_{HOMO} obtained from temperature dependent SCLC measurements, $\sigma_{tr} = \sqrt{\sigma^2_{LUMO} + \sigma^2_{HOMO}}$. Dashed lines are a guide to the eye.

improved charge transport, so it is not intuitively clear which effect dominates.

Figure 3 illustrates the kinetics of free charge recombination with all relevant states and transitions. In non-Langevin systems, there is a series of encounters (k_{enc}) and re-dissociation (k_d) events before a pair of charge carriers ultimately decay to the ground state. This can be expressed as:

$$k_{enc} n^2 = k_d n_{CT} \tag{2}$$

where n_{CT} is the equilibrium density of carriers in the CT state. It follows from Equation (2) that k_{enc} and k_d must have the same dependence on mobility, which is reasonable given that both processes are carried out by hopping in the same DOS

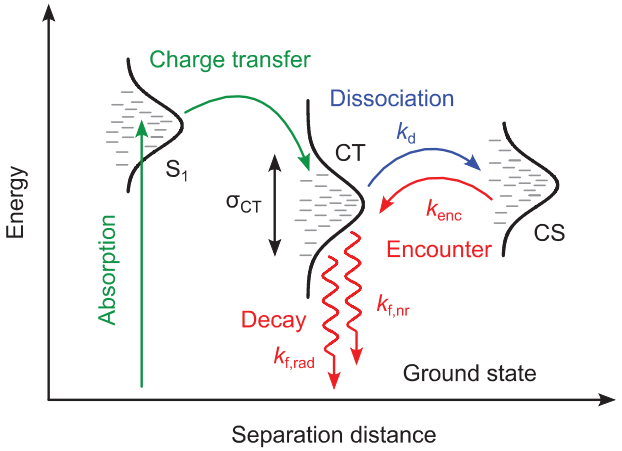

Figure 3. Schematic illustration of charge recombination in OSCs. Recombination of photo-generated charge carriers in OSCs is mediated by the interfacial CT state. The initial step of a non-geminate recombination event is the encounter of two carriers in the charge-separated (CS) state. The encounter rate (k_{enc}) is given by the carriers' mobility and may be reduced relative to the Langevin rate through geometric confinement.[39] The CT state will either dissociate to repopulate the CS state (k_d) or decay to the ground state (k_f) via radiative or non-radiative pathways. In non-Langevin systems, carriers in the CT and CS state are in quasi-equilibrium.[10] The energetic disorder leads to a broadening of both the CT and CS state, here assumed to be Gaussian in shape.

(Note S5, Supporting Information). Hence, increasing mobility by reducing energetic disorder will increase the number of encounters, but the effect will be exactly counter-balanced by the simultaneously increased probability for CT states to re-dissociate. Consequently, while no trend with mobility is expected for the recombination coefficient k_{rec}, there should be a trend for the reduction factor (see Note S6, Supporting Information). Figure S2 (Supporting Information) shows that this is indeed what we observe in our experimental data and also in data we analysed from the literature. We find that for low carrier mobilities, recombination is encounter-limited ($\gamma \approx 1$), while for high mobilities, the system is dominated by CT re-dissociation and recombination is suppressed relative to the Langevin model with γ reaching values of up to 400. The trend between reduction factor and disorder is consistent with our recent Monte Carlo simulation study, which took morphology, mobility and energetic disorder into consideration[36] as well as other works.[37,38] However, the correlation between k_{rec} and σ observed here is in clear contradiction to those simulations, which were performed under the assumption of a constant CT decay rate k_f. This clearly suggests that the disorder has a crucial influence on the decay of the CT states and thus on the overall recombination rate.

To elucidate the relationship between disorder and CT decay, we will focus in the following on the non-radiative voltage loss ΔV_{nr} as given by

$$\Delta V_{nr} = \frac{k_B T}{q} \ln\left(\frac{1}{EQE_{EL}}\right) \tag{3}$$

where EQE_{EL} is the electroluminescence (EL) quantum yield. **Figure 4** shows measured EQE_{EL} spectra representing the emission of the interfacial CT state.[40–42] We find that for all blends except PM6:Y6, the CT state has a lower energy than the emissive states in the pure D and A materials (see Figure S3, Supporting Information). Furthermore, it can be seen for the BTR:$PC_{71}BM$, NT812:$PC_{71}BM$ and thick junction PM6:Y6 systems that the change from Langevin to non-Langevin recombination via the processing conditions leads to a stronger and red-shifted CT peak. It should be noted that even in thin

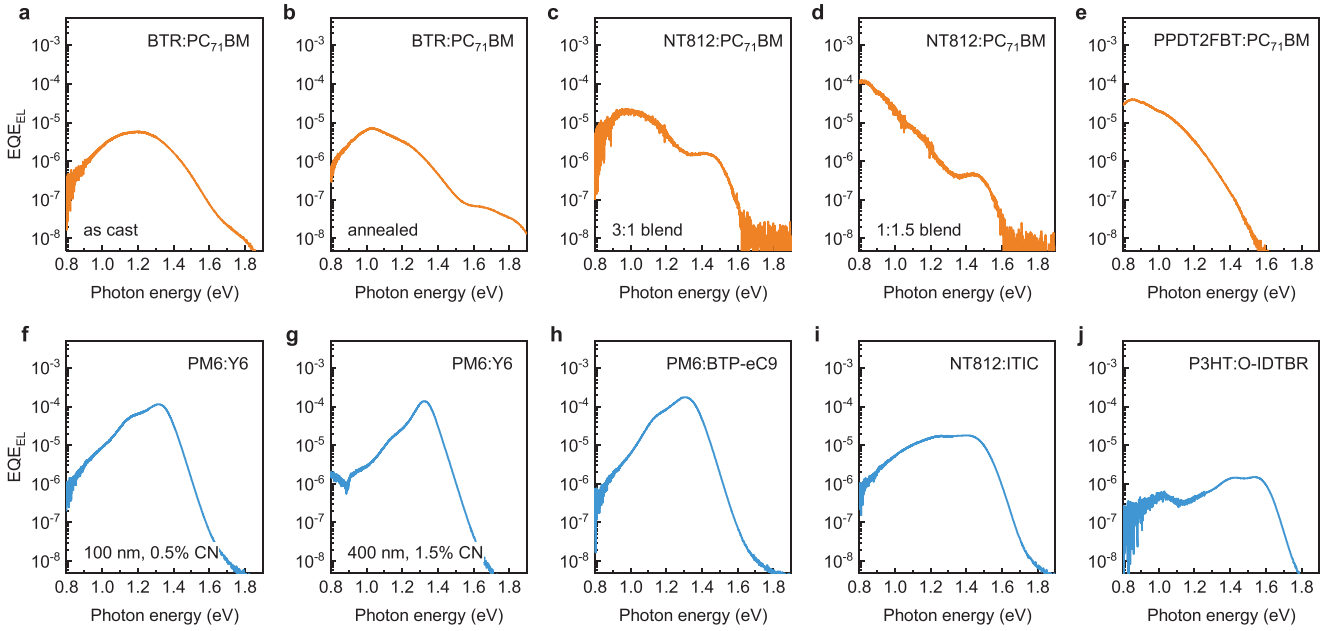

Figure 4. Electroluminescence quantum yield spectra. Measured EQE_{EL} spectra for OSCs made from the different D:A blends. The data in a–e) represents devices comprising the fullerene acceptor $PC_{71}BM$ and the data in f–j) represents devices comprising different NFAs. The EL was measured using low-injection currents (corresponding to the short-circuit current at 1-sun illumination for each system, see Table S1, Supporting Information) to ensure that the charge carriers reach thermal equilibrium before recombining.

junction PM6:Y6 even though the CT state is not observed in the EL measurements, the V_{OC} is still almost entirely determined by the energetics and kinetics of the CT state. For more details on the EL measurements and analysis, see Note S7 (Supporting Information).

Figure 5a illustrates that there is a clear correlation between the measured ΔV_{nr} values and the energetic disorder parameter σ_{tr} determined from transport measurements. For small σ_{tr} values, the voltage loss shows an initial increase but seems to saturate the systems with the largest disorder. Even more surprising, as shown in Figure 5b, there are very distinct relationships between ΔV_{nr} and the bimolecular recombination coefficient k_{rec}. While for the Langevin systems, no correlation between ΔV_{nr} and k_{rec} can be seen, the non-Langevin systems show a clear exponential dependence between the two quantities.

We first address the relationship between ΔV_{nr} and σ_{tr} (Figure 5a). It has been shown that the open-circuit voltage of OSCs is determined by properties of the interfacial CT state and, in the absence of non-thermalised carriers, can be described by[3]

$$V_{OC} = \frac{E_{CT}}{q} - \frac{k_B T}{q} \ln\left(\frac{k_f N_{CT}}{G}\right) \quad (4)$$

where E_{CT} is the energy of the CT state, N_{CT} the density of D:A interfaces, and G the generation rate of free charge carriers. The total CT state decay rate can be written as a sum of radiative and non-radiative channels, $k_f = k_{f,rad} + k_{f,nr}$, with EQE_{EL} being a proxy for the ratio between the radiative and the total decay rate. In an ideal solar cell, only radiative recombination (which is inevitable) occurs and EQE_{EL} equals unity. However, with EQE_{EL} values between 10^{-7} and 10^{-5}, we find that non-radiative recombination clearly dominates and $k_f \approx k_{f,nr}$. Next, we recall that the CT-to-ground-state decay is an electron transfer process. Therefore, $k_{f,nr}$ can be described in the framework of the semi-classical Marcus model or, if the coupling to high-frequency

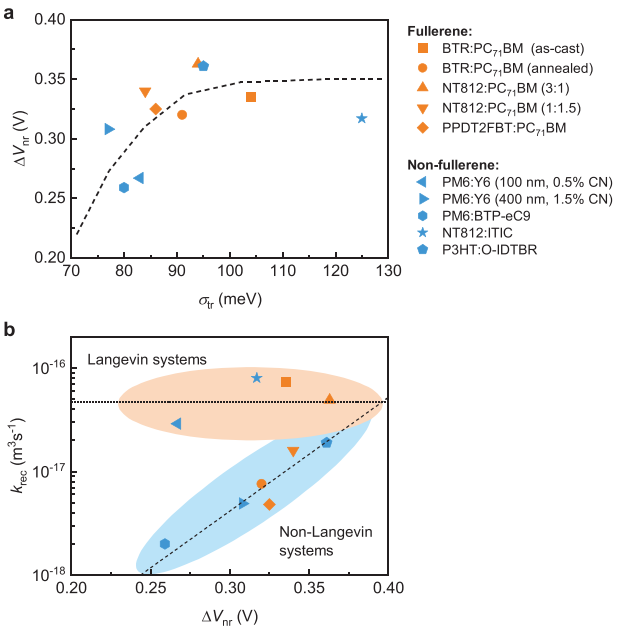

Figure 5. Non-radiative voltage loss and its interrelations. a) Non-radiative voltage loss ΔV_{nr} determined from the measured EQE_{EL} according to Equation (3) as a function of energetic disorder. b) Recombination coefficient k_{rec} as a function of ΔV_{nr}. For the non-Langevin systems ($\gamma \gg 1$), a clear correlation between k_{rec} and ΔV_{nr} can be seen. No such correlation is apparent for the Langevin systems ($\gamma \approx 1$), where the assumption of quasi-equilibrium between free carriers and CT states does not hold.

vibrational modes is considered, the Marcus–Levich–Jortner model. Both models account only for the dynamic disorder, that is, the coupling to vibrational modes, which is given by $\sigma_D^2 = 2k_B T\lambda$, where λ is the reorganisation energy. However, as detailed in Note S8 (Supporting Information), they can be extended to account for static disorder by substituting σ_D^2 with the total disorder $\sigma_T^2 = \sigma_S^2 + \sigma_D^2$. Upon considering static disorder, the semiclassical Marcus formula reads[2,19,43]

$$k_{f,nr} = \frac{2\pi}{\hbar}|V_{el}|^2 \frac{1}{\sqrt{2\sigma_T^2}} \exp\left(-\frac{(\lambda - E_{CT})^2}{2\sigma_T^2}\right) \quad (5)$$

where V_{el} is the electronic coupling between the CT state and the ground state. We note that in contrast to $k_{f,nr}$, the radiative rate constant $k_{f,rad}$ is only slightly affected by σ_S. Therefore, according to Equations (3)–(5), it is $k_{f,nr}$ that defines the dependence of ΔV_{nr} on σ_S. According to previous theoretical work,[22] $k_{f,nr}$ (and thus ΔV_{nr}) sharply increases with σ_S when the disorder is small and reaches a plateau at large σ_S values. Finally, we note that the static disorder parameter σ_S that enters in Equation (5) and the corresponding Marcus–Levich–Jortner equation (see Note S8, Supporting Information) and the parameter $\sigma_{tr}^2 = \sigma_{HOMO}^2 + \sigma_{LUMO}^2$ used above for the discussion of charge transport are interrelated. The static disorder responsible for the broadening of the CT states can be written as $\sigma_S^2 = \sigma_{HOMO}^2 + \sigma_{LUMO}^2 + \sigma_{el}^2$, where σ_{el} is the width of the electrostatic interaction energy distribution for holes and electrons at the D:A interface.[22] Thus, a larger σ_{tr} in general would mean also a larger σ_s, which together with Equations (3)–(5) explains the trend between ΔV_{nr} and σ_{tr} in Figure 5a. Further evidence for the importance of static disorder comes from the injection dependent EQE_{EL} measurements (see Figure S4, Supporting Information). It is observed that increasing the injection current leads to the emergence and/or enhancement of the (D or A) exciton feature, while there is a decrease in the intensity of the CT peak. One explanation for such observations is thermal population due to carrier heating. However, as these systems posess a high carrier density (since recombination is slow), we assign the behaviour in our EL data to a signature of state filling occurring in the presence of static disorder.

We now turn to the correlation between k_{rec} and ΔV_{nr} (Figure 5b). Following the kinetic model outlined in Note S5 (Supporting Information), quasi-equilibrium between CT states and free charges in the CS state implies that the recombination coefficient k_{rec} can be linked to the CT decay rate via

$$k_{rec} = \frac{k_f}{k_d + k_f} k_{enc} \quad (6)$$

For the discussion here, the most relevant parameter in Equation (6) is the overall decay rate of the CT state to the ground state, $k_f = k_{f,rad} + k_{f,nr}$, which defines the lifetime of the CT state. As mentioned above, in organic systems k_f is dominated by non-radiative decay channels, $k_f \approx k_{f,nr}$, which is also evident from the observed EQE_{EL} values between 10^{-7} and 10^{-5}, see Figure 4, Table 1. From Equation (3) to (6), a general trend between k_{rec} and ΔV_{nr} is expected if quasi-equilibrium between CT and CS states prevails. In D:A blends with short-lived CT states (large $k_{f,nr}$), bimolecular recombination is diffusion-limited (Langevin systems, $k_{rec} \approx k_L$), meaning that every pair of free carriers forming a CT state will recombine. Thus, in this case, k_{rec} and ΔV_{nr} are uncorrelated, as the recombination rate is solely given by the carriers' encounter rather than the kinetics of the formed CT state. In contrast, in the case of long-lived CT states, $k_{rec} \approx k_{f,nr}/k_d$, indicating that k_{rec} should depend on disorder. Thus, for the non-Langevin systems, the only parameter common between k_{rec} and ΔV_{nr} is the non-radiative CT decay rate, and the reduction in recombination losses is due to a reduced $k_{f,nr}$ (i.e., a longer CT lifetime) rather than the energy or the total density of the CT states.

Thus, our data for the first time experimentally shows for a range of D:A blends, including the latest NFA-based systems, the simultaneous reduction of k_{rec} and ΔV_{nr} with the reduced (static) disorder as previously theoretically suggested.[22] The theoretical work by Coropceanu and Brédas employed molecular dynamics simulations combined with density functional theory calculations on P3HT:PCBM. The calculations evaluated the impact of static and dynamic disorders. The radiative and non-radiative transition rates were also evaluated and it was found that even a small amount of static disorder can have a very large negative impact on the non-radiative recombination rates (due to its exponential dependence). These findings are also in line with recent work by Vandewal and co-workers[44] showing a relationship between non-radiative recombination, reorganisation energy and the spectral width of the EL emission, as well as earlier work relating the CT decay time with photoluminescence quantum yield.[10,45] Moreover, our data show that such a correlation between voltage loss, recombination and disorder does not exist for Langevin systems with a fast CT decay (since recombination is diffusion limited), as indicated by the plateau regions in Figure 5.

The connections drawn herein between k_{rec} and ΔV_{nr} through the CT decay rate k_f indicate that reducing energetic disorder is an important prerequisite to gain in the FF and V_{OC} concomitantly. It should be noted that even though the CT lifetime consists of the decay rate (k_f) of the CT state and its dissociation rate (k_d) to free carriers, V_{OC} is independent of the CT dissociation or free carrier encounter rate constant (k_{enc}). Following the same line or arguments, it is also important to note that a prolonged carrier lifetime does not necessarily result in an increased V_{OC}. Rather, the V_{OC} only depends on the decay of the CT state to the ground state (and other properties of the CT state). Indeed, decreasing k_{enc} or increasing k_d will result in a long carrier lifetime, but will have no effect on V_{OC} as long as the CT state decay rate constant k_f remains unchanged. Thus, in order to simultaneously improve both the FF and the V_{OC}, k_f must be reduced.

Whilst in this work we demonstrated some active layer engineering strategies for mitigating energetic disorder, other approaches such as creating vertical segregation or use of ternary systems are also effective methods to reduce energetic disorder. In terms of material design strategies, although the material design strategy to effectively lower the energetic disorder of OSCs is not yet perfectly clear, studies have however shown that precise control of the structure of organic materials can be a direct and effective method; the energetic disorder can be influenced by structural features of organic materials

through high crystallinity, good molecular rigidity and small reorganization energy. For instance, materials that contain conjugated macrocyclic units usually possess strong crystallinity. The rational introduction of non-covalent interaction could effectively fine-tune the molecular planarity and crystallinity properties. In addition, previous work in agreement with experimental data presented here has suggested that sphere-like fullerenes, or molecules generally, can induce unfavorable electrostatic hole–electron interactions which contribute to the static disorder.[46,47]

3. Conclusion

In conclusion, we have investigated the relationship between energetic disorder and non-radiative charge recombination in organic solar cells. From an extensive experimental study based on a range of fullerene and non-fullerene organic solar cell systems, we find that reducing static energetic disorder is the key to reducing free-carrier recombination and non-radiative voltage losses, leading to a simultaneous improvement of the fill factor and open-circuit voltage. Using the modified Marcus–Levich–Jortner model, we postulate that the underlying mechanism is an interrelation between the decay rate of the interfacial CT state and the broadening of the DOS experienced by carriers in the CT manifold; a narrower distribution, that is, less energetic disorder, results in a slower (non-radiative) decay of the CT state. This results in reduced non-radiative recombination and with this, total CT recombination. Therefore, minimising energetic disorder is a critical design criterion for further increasing the performance of organic solar cells and ultimately breaking the 20% efficiency limit. Systematic reduction of disorder, for example through suitable adaptation of the morphology in terms of aggregation and conformation, has the potential to simultaneously improve charge transport and reduce recombination and voltage losses.

4. Experimental Section

Materials: All photoactive materials were purchased from 1-Material, except for NT812 and PPDT2FBT that were synthesised according to previous reports.[48,49]

Devices: The device structure of solar cells is indium tin oxide (ITO)/poly(3,4-ethylenedioxythiophene)-poly(styrenesulfonate) (PEDOT:PSS)/active layer/cathode. Devices were prepared on patterned ITO-covered glass substrates that were pre-cleaned with detergent, deionized water, acetone, and 2-propanol in an ultrasonic bath and treated with oxygen plasma at room temperature. PEDOT:PSS was spin-coated in ambient air and annealed at 150 °C for 15 min. The active layer was prepared by dissolving the D and A in a common solvent and spin coating the blend solution in a nitrogen-filled glove box. The cathode consists of either a solvent-processed or vapour-deposited electron-transport layer and a thermally evaporated metal electrode. Details on the processing of the individual blends and the preparation of the cathode depending on the blend system can be found in Note S1 (Supporting Information). For electron-only devices, the PEDOT:PSS layer was replaced by ZnO nanoparticles dissolved in 2-propanol (Avantama N-10) that were spin-coated in ambient air and annealed at 120 °C for 30 min. For hole-only devices, the cathode was replaced by 20 nm of MoO_3 and 100 nm of Au that was thermally evaporated on top of the blend layers. The effective area of the devices was 0.06 $cm^{[2]}$ for *J–V* and EL measurements and 0.011 $cm^{[2]}$ for BACE measurements (which was measured by Dektak, the Bruker model).

Current–voltage measurements: *J–V* curves were measured at room temperature inside a glove box with a Keithley 2400 source measuring unit in a two-wire configuration. Simulated AM1.5G illumination at 100 mW cm^{-2} was provided by a filtered Oriel Class AAA Xenon lamp calibrated with a KG5-filtered Si solar cell (certified by Fraunhofer ISE). The light intensity was continuously monitored with a Si photodiode. For temperature-dependent *J–V* measurements, samples were placed in a liquid nitrogen cryostat. Details of the analysis of temperature-dependent SCLCs are given in Note S3 (Supporting Information).

Bias-assisted charge extraction (BACE): To establish steady-state conditions, a high-power (1 W) 638-nm laser diode (InsaneWare) with a switch-off time of 10 ns was used. The laser diode was operated at 500 Hz with a duty cycle of 50%. A pulse generator (Agilent 81150A) was used to apply the pre-bias (matching V_{OC}) and collection bias voltage, which were amplified by a home-built amplifier allowing for fast extraction times of 10–20 ns. The current transients were measured over a 10 Ω resistor in series with the sample and recorded with an oscilloscope (Agilent DSO9104H). More details of the measurement principle can be found in Note S2 (Supporting Information).

Electroluminescence: EL spectra were acquired using a spectrometer (Andor SR393i-B) equipped with a thermoelectrically cooled Si CCD sensor (iDus DU420A BR-DD) and InGaAs photodiode array (iDus DU491A-1.7). The voltage was applied to the devices using a Keithley 2400 source measuring unit, and the spectra were collected at different injection currents. All measurements were spectrally calibrated using a halogen lamp with a known spectral irradiance. The normalised EL spectra were scaled to absolute values by a separate calibration measurement, where the absolute photon flux was measured with a calibrated Si photodiode for the same injection conditions. The EL quantum yield was calculated based on the total number of emitted photons and the number of injected charges. More details on the determination of EQE_{EL} and ΔV_{nr} can be found in Note S6 (Supporting Information).

Code Availability: To determine the energetic disorder, we used the open-source program https://github.com/mkemerink/FitSCLC.

Supporting Information

Supporting Information is available from the Wiley Online Library or from the author.

Acknowledgements

This work was supported by the Alexander von Humboldt Foundation and the Deutsche Forschungsgemeinschaft (DFG, German Research Foundation) through the project Fabulous (NE 410/20, SH 1669/1-1). S.S. thanks Dieter Neher (University of Potsdam) for fruitful discussions and access to laboratories. H.Y.W. acknowledges financial support from the National Research Foundation of Korea (grants NRF2020M3H4A3081814 and 2019R1A6A1A11044070). S.W. acknowledges funding from the European Union's Horizon 2020 research and innovation programme under the Marie Skłodowska-Curie grant agreement No 799801 ("ReMorphOPV"). V.C. acknowledges funding by the Office of Naval Research under award No N00014-20-1-2110 and the University of Arizona.

Open access funding enabled and organized by Projekt DEAL.

Conflict of Interest

The authors declare no conflict of interest.

Data Availability Statement

The data that support the findings of this study are available from the corresponding author upon reasonable request.

Keywords

energetic disorder, non-radiaive decay, reduced recombination

Received: October 21, 2022
Revised: December 3, 2022
Published online:

[1] J. Zhang, H. S. Tan, X. Guo, A. Facchetti, H.e Yan, *Nat. Energy* **2018**, *3*, 720.
[2] S. Xie, Y. Xia, Z. Zheng, X. Zhang, J. Yuan, H. Zhou, Y. Zhang, *Adv. Funct. Mater.* **2018**, *28*, 1705659.
[3] A. Armin, W. Li, O. J. Sandberg, Z. Xiao, L. Ding, J. Nelson, D. Neher, K. Vandewal, S. Shoaee, T. Wang, H. Ade, T. Heumuller, C. Brabec, P. Meredith, *Adv. Energy Mater.* **2021**, *11*, 2003570.
[4] N. Tokmoldin, J. Vollbrecht, S. M. Hosseini, B. Sun, L. Perdigon-Toro, H. Y. Woo, Y. Zou, D. Neher, S. Shoaee, *Adv. Energy Mater.* **2021**, *11*, 2100804.
[5] T. R. Andersen, H. F. Dam, M. Hosel, M. Helgesen, J. E. Carle, T. T. Larsen-Olsen, S. A. Gevorgyan, J. W. Andreasen, J. Adams, N. Li, F. Machui, G. D. Spyropoulos, T. Ameri, Noella Lemaitre, M. Legros, A. Scheel, D. Gaiser, K. Kreul, S. Berny, O. R. Lozman, S. Nordman, M. Valimaki, M. Vilkman, R. R. Sondergaard, M. Jorgensen, C. J. Brabec, F. C. Krebs, *Energy Environ. Sci.* **2014**, *7*, 2925.
[6] A. Köhler, H. Bässler, *Electronic Processes in Organic Semiconductors: An Introduction*, Wiley-VCH Verlag GmbH & Co., Weinheim, Germany **2015**.
[7] A. Armin, J. R. Durrant, S. Shoaee, *J. Phys. Chem. C* **2017**, *121*, 13969.
[8] A. Armin, J. Subbiah, M. Stolterfoht, S. Shoaee, Z. Xiao, S. Lu, D. J. Jones, P. Meredith, *Adv. Energy Mater.* **2016**, *6*, 1600939.
[9] S. Wilken, D. Scheunemann, S. Dahlström, M. Nyman, J. Parisi, R. Österbacka, *Adv. Electron. Mater.* **2021**, *7*, 2001056.
[10] T. M. Burke, S. Sweetnam, K. Vandewal, M. D. McGehee, *Adv. Energy Mater.* **2015**, *5*, 1500123.
[11] S. Shoaee, A. Armin, M. Stolterfoht, S. M. Hosseini, J. Kurpiers, D. Neher, *Sol. RRL* **2019**, *3*, 1900184.
[12] S. Wilken, In *Charge Recombination in Organic Solar Cells*, Soft-Matter Thin Film Solar Cells: Physical Processes and Device Simulation (Eds: J. Ren, Z. Kan), AIP Publishing, Melville, NY **2020**.
[13] J. Benduhn, K. Tvingstedt, F. Piersimoni, S. Ullbrich, Y. Fan, M. Tropiano, K. A. Mcgarry, O. Zeika, M. K. Riede, C. J. Douglas, S. Barlow, S. R. Marder, D. Neher, D. Spoltore, K. Vandewal, *Nat. Energy* **2017**, *2*, 17053.
[14] M. Azzouzi, J. Yan, T. Kirchartz, K. Liu, J. Wang, H. Wu, J. Nelson, *Phys. Rev. X* **2018**, *8*, 31055.
[15] X.-K. Chen, D. Qian, Y. Wang, T. Kirchartz, W. Tress, H. Yao, J. Yuan, M. Hulsbeck, M. Zhang, Y. Zou, Y. Sun, Y. Li, J. Hou, O. Inganäs, V. Coropceanu, J.-L. Brédas, F. Gao, *Nat. Energy* **2021**, *6*, 799.
[16] J. C. Blakesley, D. Neher, *Phys. Rev. B* **2011**, *84*, 075210.
[17] M. Panhans, S. Hutsch, J. Benduhn, K. S. Schellhammer, V. C. Nikolis, T. Vangerven, K. Vandewal, F. Ortmann, *Nat. Commun.* **2020**, *11*, 1488.
[18] K. Tvingstedt, J. Benduhn, K. Vandewal, *Mater. Horiz.* **2020**, *7*, 1888.
[19] F.-J. Kahle, A. Rudnick, H. Bässler, A. Köhler, *Mater. Horiz.* **2018**, *5*, 837.
[20] T. Linderl, T. Zechel, A. Hofmann, T. Sato, K. Shimizu, H. Ishii, W. Brütting, *Phys. Rev. Appl.* **2020**, *13*, 24061.
[21] C. Göhler, M. Saladina, Y. Wang, D. Spoltore, J. Benduhn, K. Leo, C. Deibel, *Phys. Rev. Appl.* **2021**, *15*, 64009.
[22] Z. Zheng, N. R. Tummala, T. Wang, V. Coropceanu, J. L. Brédas, *Adv. Energy Mater.* **2019**, *9*, 1803926.
[23] T. Upreti, S. Wilken, H. Zhang, M. Kemerink, *J. Phys. Chem. Lett.* **2021**, *12*, 9874.
[24] T. Wang, V. Coropceanu, J.-L. Brédas, *Chem. Mater.* **2019**, *31*, 6239.
[25] V. Coropceanu, J.-L. Brédas, S. Mehraeen, *J. Phys. Chem. C* **2017**, *121*, 24954.
[26] J. Yan, E. Rezasoltani, M. Azzouzi, F. Eisner, J. Nelson, *Nat. Commun.* **2021**, *12*, 3642.
[27] S. Wilken, T. Upreti, A. Melianas, S. Dahlström, G. Persson, E. Olsson, R. Österbacka, M. Kemerink, *Sol. RRL* **2020**, *4*, 2000029.
[28] A. Armin, Z. Chen, Y. Jin, K. Zhang, F. Huang, S. Shoaee, *Adv. Energy Mater.* **2018**, *8*, 1701450.
[29] S. M. Hosseini, N. Tokmoldin, Y. W. Lee, Y. Zou, H. Y. Woo, D. Neher, S. Shoaee, *Sol. RRL* **2020**, *4*, 2000498.
[30] N. Felekidis, A. Melianas, M. Kemerink, *Org. Electron.* **2018**, *61*, 318.
[31] W. F. Pasveer, J. Cottaar, C. Tanase, R. Coehoorn, P. A. Bobbert, P. W. M. Blom, D. M. de Leeuw, M. A. J. Michels, *Phys. Rev. Lett.* **2005**, *94*, 206601.
[32] A. Melianas, N. Felekidis, Y. Puttisong, S. C. J. Meskers, O. Inganäs, W. M. Chen, M. Kemerink, *Proc. Natl. Acad. Sci. U. S. A.* **2019**, *116*, 23416.
[33] T. Upreti, Y. Wang, H. Zhang, D. Scheunemann, F. Gao, M. Kemerink, *Phys. Rev. Appl.* **2019**, *12*, 064039.
[34] D. Neher, J. Kniepert, A. Elimelech, L. J. A. Koster, *Sci. Rep.* **2016**, *6*, 24861.
[35] S. Shoaee, M. Stolterfoht, D. Neher, *Adv. Energy Mater.* **2018**, *8*, 1703355.
[36] G. Zuo, S. Shoaee, M. Kemerink, D. Neher, *Phys. Rev. Appl.* **2021**, *16*, 34027.
[37] S. N. Hood, I. Kassal, *J. Phys. Chem. Lett.* **2016**, *7*, 4495.
[38] A. Karki, G. J. A. H. Wetzelaer, G. N. M. Reddy, V. Nádaždy, M. Seifrid, F. Schauer, G. C. Bazan, B. F. Chmelka, P. W. M. Blom, T. Q. Nguyen, *Adv. Funct. Mater.* **2019**, *29*, 1901109.
[39] M. C. Heiber, C. Baumbach, V. Dyakonov, C. Deibel, *Phys. Rev. Lett.* **2015**, *114*, 136602.
[40] K. Vandewal, K. Tvingstedt, A. Gadisa, O. Inganäs, J. V. Manca, *Phys. Rev. B* **2010**, *81*, 125204.
[41] K. Vandewal, K. Tvingstedt, A. Gadisa, O. Inganäs, J. V. Manca, *Nat. Mater.* **2009**, *8*, 904.
[42] K. Tvingstedt, K. Vandewal, A. Gadisa, F. Zhang, J. Manca, O. Inganäs, *J. Am. Chem. Soc.* **2009**, *131*, 11819.
[43] T. Unger, S. Wedler, F.-J. Kahle, U. Scherf, H. Bässler, A. Köhler, *J. Phys. Chem. C* **2017**, *121*, 22739.
[44] Q. Liu, S. Smeets, S. Mertens, Y. Xia, A. Valencia, J. D'Haen, W. Maes, K. Vandewal, *Joule* **2021**, *5*, 2365.
[45] Y. Liu, Z. Zheng, V. Coropceanu, J.-L. Brédas, D. S. Ginger, *Mater. Horiz.* **2021**, *9*, 325.
[46] T. Wang, M. K. Ravva, J.-L. Brédas, *Adv. Funct. Mater.* **2016**, *26*, 5913.
[47] M. K. Ravva, T. Wang, J.-L. Brédas, *Chem. Mater.* **2016**, *28*, 8181.
[48] Y. Jin, Z. Chen, S. Dong, N. Zheng, L. Ying, X.-F. Jiang, F. Liu, F. Huang, Y. Cao, *Adv. Mater.* **2016**, *28*, 9811.
[49] S.-J. Ko, B. Walker, T. L. Nguyen, H. Choi, J. Seifter, M. A. Uddin, T. Kim, S. Kim, J. Heo, G.i-H. Kim, S. Cho, A. J. Heeger, H. Y. Woo, J. Y. Kim, *Adv. Funct. Mater.* **2016**, *26*, 3324.